



# Altered Topological Properties of Gray Matter Structural Covariance Networks in Minimal Hepatic Encephalopathy

Tian-Xiu Zou<sup>1†</sup>, Lilan She<sup>1†</sup>, Chuanyin Zhan<sup>1†</sup>, Yong-Qing Gao<sup>1,2</sup> and Hua-Jun Chen<sup>1\*</sup>

<sup>1</sup>Department of Radiology, Fujian Medical University Union Hospital, Fuzhou, China, <sup>2</sup>Department of Radiology, Fuqing City Hospital, Fuqing, China

**Background and Aims:** Liver cirrhosis commonly induces brain structural impairments that are associated with neurological complications (e.g., minimal hepatic encephalopathy (MHE)), but the topological characteristics of the brain structural network are still less well understood in cirrhotic patients with MHE. This study aimed to conduct the first investigation on the topological alterations of brain structural covariance networks in MHE.

**Methods:** This study included 22 healthy controls (HCs) and 22 cirrhotic patients with MHE. We calculated the gray matter volume of 90 brain regions using an automated anatomical labeling (AAL) template, followed by construction of gray matter structural covariance networks by thresholding interregional structural correlation matrices as well as graph theoretical analysis.

**Results:** MHE patients showed abnormal small-world properties of the brain structural covariance network, i.e., decreased clustering coefficient and characteristic path length and lower small-worldness parameters, which indicated a tendency toward more random architecture. In addition, MHE patients lost hubs in the prefrontal and parietal regions, although they had new hubs in the temporal and occipital regions. Compared to HC, MHE patients had decreased regional degree/betweenness involving several regions, primarily the prefrontal and parietal lobes, motor region, insula and thalamus. In addition, the MHE group also showed increased degree/betweenness in the occipital lobe and hippocampus.

**Conclusion:** These results suggest that MHE leads to altered coordination patterns of gray matter morphology and provide structural evidence supporting the idea that MHE is a neurological complication related to disrupted neural networks.

**Keywords:** minimal hepatic encephalopathy, small-world network, graph theory, brain structural network, gray matter volume

**Abbreviations:**  $\gamma$ , normalized clustering coefficient;  $\lambda$ , normalized path length;  $\sigma$ , small-worldness; AAL, automated anatomical labeling;  $C_p$ , clustering coefficient; FDA, functional data analysis;  $L_p$ , characteristic path length; MHE, Minimal hepatic encephalopathy; PHES, Psychometric Hepatic Encephalopathy Score; RGMV, regional gray matter volume.

## OPEN ACCESS

### Edited by:

Angel Acebes,  
Centro de Investigaciones  
Biomédicas de Canarias (CIBICAN),  
Spain

### Reviewed by:

Miguel Ángel García-Cabezas,  
Boston University, United States  
Joachim H. R. Lübke,  
Forschungszentrum Jülich,  
Helmholtz-Gemeinschaft Deutscher  
Forschungszentren (HZ), Germany

### \*Correspondence:

Hua-Jun Chen  
chj0075@126.com

<sup>†</sup>These authors have contributed  
equally to this work

**Received:** 01 September 2018

**Accepted:** 15 November 2018

**Published:** 28 November 2018

### Citation:

Zou T-X, She L, Zhan C, Gao Y-Q  
and Chen H-J (2018) Altered  
Topological Properties of Gray Matter  
Structural Covariance Networks in  
Minimal Hepatic Encephalopathy.  
*Front. Neuroanat.* 12:101.  
doi: 10.3389/fnana.2018.00101

## INTRODUCTION

Previous studies have shown that brain structural abnormalities commonly occur in cirrhotic patients. Neuropathological studies have documented the loss of brain parenchyma due to cirrhosis (Krill and Butterworth, 1997). Among patients with hepatic dysfunction, neuronal cell loss (probably due to chronic portosystemic shunting and ammonia exposure) has been associated with liver failure (Butterworth, 2007). *In vivo* studies using computed tomography and magnetic resonance imaging (MRI) also reveal diffuse brain atrophy in cirrhosis (Tarter et al., 1986; Zeneroli et al., 1987, 1991; Iwasa et al., 2012), which progresses with advanced liver disease (Guevara et al., 2011).

Minimal hepatic encephalopathy (MHE) is a common complication of liver cirrhosis and is characterized by a wide range of mild neurocognitive impairments, such as slowing of psychomotor activity, attention deficits, impairment of memory, and decreased executive abilities (Bajaj et al., 2009), which in turn negatively influence daily activities and are often associated with poor prognosis (Stewart and Smith, 2007). Although MHE is traditionally considered to be a disease related to brain dysfunction, its neuropathological mechanisms remain unclear. New findings suggest that brain structural impairments may play another important role in MHE. Patients with MHE showed more serious brain atrophy as compared with those without MHE (Guevara et al., 2011). A previous study has suggested that structural alterations are associated with lower psychometric performance of cirrhotic patients (Amodio et al., 2003).

Despite the above findings in cirrhotic patients with MHE, previous studies have only focused on regional structural changes in cirrhosis and did not consider brain network-level architecture (i.e., topological organization). Recent progress in structural MRI analysis has facilitated the development of a human brain structural network model that is based on statistical correlations of morphological descriptors, including the thickness of the cortex or regional gray matter volume (RGMV; He et al., 2007; Wu et al., 2012). This type of brain network possesses small-world properties (He et al., 2007; Lv et al., 2010; that feature extensive local clustering and short path lengths that link each network node; Watts and Strogatz, 1998), thereby making it an attractive model for evaluating complex brain networks because it allows specialized, as well as integrated, information processing and maximizes information propagation efficiency using minimal wiring costs (Sporns et al., 2005; Achard and Bullmore, 2007). Gray matter structural associations have been shown to reflect neurological dysfunctions (Dazzan et al., 2004) and are correlated with functional connectivity (Bhojraj et al., 2010). Importantly, topological analysis of the brain structural network can provide new insights into various neurological diseases such as schizophrenia (Shi et al., 2012) and Alzheimer's disease (Yao et al., 2010) and the normal aging process (Zhu et al., 2012), which all induce a disrupted integrity of brain functional networks. Moreover, the impaired small-world efficiency in the structural cortical

network has been found to be associated with neurological disease progression (He et al., 2009). The abovementioned studies have also shown the study populations with either neurological diseases or aging exhibited considerable brain structural changes (Wen et al., 2011). Thus, it is hypothesized that the brain structural networks of MHE patients could exhibit large-scale topological alterations, as these patients have been found to have diffuse gray and white matter atrophy (Guevara et al., 2011; Iwasa et al., 2012; Montoliu et al., 2012).

Actually, MHE has been demonstrated as a neurological disease that is related to abnormal brain networks. MHE patients could exhibit altered functional connectivity involving various intrinsic brain networks, including those of dorsal attention, visual, auditory and default-mode (Qi et al., 2012). In addition, changes involving whole-brain functional connectivity have been reported in MHE patients (Zhang et al., 2012). Notably, based on the resting-state fMRI, it has been suggested that MHE is associated with decreased brain small-world network efficiency (Hsu et al., 2012). In these contexts, we aimed to make the first investigation on the topological alterations involving brain structural covariance networks in MHE patients, which can provide morphological insights into MHE mechanisms that may coincide with functional findings.

## MATERIALS AND METHODS

### Subjects

The Research Ethics Committee of the Fujian Medical University Union Hospital, China approved this study, and each study participant provided written informed consent. This study involved total of 22 MHE cirrhotic patients and 22 healthy controls (HCs). The two groups were matched in terms of age, sex and education level. **Table 1** shows the demographical data of the study participants. Liver cirrhosis was diagnosed based on biopsy (4/22) or individual history, biochemical and physical examination, as well as imaging such as ultrasound and computed tomography (18/22). Neuropsychological tests, namely, Psychometric Hepatic Encephalopathy Score (PHES) examination, were performed to assess MHE, which included a digit symbol test, number connection tests A and B, serial dotting, as well as line tracing. Details on how to diagnose MHE have been described previously (Chen et al., 2015). None of the participant developed neuropsychiatric disorders, received psychotropic medications, or was diagnosed with other uncontrolled endocrine or metabolic disorders (e.g., diabetes mellitus and thyroid dysfunction), or took excessive amounts of alcohol for 6 months before the study.

### MRI Acquisition

MRI scanning was performed using a 3.0 T scanner (Siemens, Verio, Germany). Three-dimensional T1-weighted sagittal images of magnetization-prepared rapid gradient echo (MPRAGE) were obtained using the following settings: TR = 1.9 ms, TE = 2.48 ms, FOV = 256 mm × 256 mm,

**TABLE 1** | Demographic and clinical features of the study participants.

|   | HCs subjects (n = 22) | MHE patients (n = 22) | P value                |
|---|-----------------------|-----------------------|------------------------|
| Age (years)   | 51.8 ± 6.5            | 51.3 ± 8.9            | 0.848                  |
| Sex (male/female)   | 15/7                  | 17/5                  | 0.498 ( $\chi^2$ test) |
| Education level (years)                                     | 8.7 ± 2.2             | 8.8 ± 2.7             | 0.812                  |
| Etiology of cirrhosis (HBV/alcoholism/HBV+alcoholism/other) | -                     | 13/4/2/3              | -                      |
| Child-Pugh stage (A/B/C)                                    | -                     | 3/13/6                | -                      |
| Final PHES score  | 0.7 ± 2.2             | -8.2 ± 3.0            | <0.001                 |
| Number connection test A (s)                                | 37.0 ± 12.3           | 57.3 ± 17.3           | <0.001                 |
| Number connection test B (s)                                | 63.8 ± 29.2           | 134.2 ± 62.3          | <0.001                 |
| Serial dotting test (s)                                     | 43.0 ± 7.6            | 65.3 ± 18.5           | <0.001                 |
| Digit symbol test (raw score)                               | 45.2 ± 9.3            | 26.9 ± 8.5            | <0.001                 |
| Line tracing test (raw score)                               | 115.8 ± 16.1          | 192.3 ± 47.3          | <0.001                 |

matrix = 256 × 256, flip angle = 9°, slice thickness = 1.0 mm, 176 slices.

## Measurements of Regional Gray Matter Volume (RGMV)

The structural images were preprocessed using a voxel-based morphometry (VBM) toolbox as implemented in Statistical Parametric Mapping software (SPM8)<sup>1</sup>. Structural images were segmented to the GM, white matter, as well as cerebrospinal fluid. High-dimensional normalization was performed using the diffeomorphic anatomical registration using exponentiated lie algebra (DARTEL) approach (Ashburner, 2007) and then the segmented images were submitted to the Montreal Neurological Institute (MNI). We applied tissue deformation for modulation of the segmented GM images. Then, the entire gray matter was parcellated into 45 regions per hemisphere (a total of 90 regions, **Table 2**) as described by the automated anatomical labeling (AAL) atlas (Tzourio-Mazoyer et al., 2002), for

<sup>1</sup><https://www.fil.ion.ucl.ac.uk/spm/>

RGMV estimation of each subject. Linear regression analysis was performed to exclude the effects of age, gender, as well as education level. The regression residuals were then substituted for the raw RGMV and designated as the corrected RGMV.

## Construction of Brain Structural Covariance Network

In the present study, the structural connections involving the whole-brain network were described using statistical correlations between pairs of the corrected RGMV. For every group, Pearson correlation coefficients between corrected RGMV were calculated across each study participant to generate the interregional correlation matrix ( $N \times N$ , where  $N$  represents the number of gray matter areas, here  $N = 90$ ). Then, the correlation matrix of every group was thresholded into a binary matrix and converted into an undirected graphical diagram (network; **Figure 1**). The constructed interregional correlation matrices were thresholded across various network densities

**TABLE 2** | Abbreviations of various automated anatomical labeling (AAL) regions.

| Abbreviation | AAL region                                | Abbreviation | AAL region  |
|--------------|---|--------------|---|
| AMYG         | Amygdala                                  | MOG          | Middle occipital gyrus                                |
| ANG          | Angular gyrus                             | SOG          | Superior occipital gyrus                              |
| CAL          | Calcarine fissure and surrounding cortex  | OLF          | Olfactory cortex                                      |
| CAU          | Caudate nucleus                           | PAL          | Lenticular nucleus, pallidum                          |
| ACG          | Anterior cingulate and paracingulate gyri | PCL          | Paracentral lobule                                    |
| DCG          | Median cingulate and paracingulate gyri   | PHG          | Parahippocampal gyrus                                 |
| PCG          | Posterior cingulate gyrus                 | IPL          | Inferior parietal, but supramarginal and angular gyri |
| CUN          | Cuneus                                    | SPG          | Superior parietal gyrus                               |
| IFGoperc     | Inferior frontal gyrus, opercular part    | PoCG         | Postcentral gyrus                                     |
| ORBinf       | Inferior frontal gyrus, orbital part      | PreCG        | Precentral gyrus                                      |
| IFGtriang    | Inferior frontal gyrus, triangular part   | PCUN         | Precuneus   |
| ORBsupmed    | Superior frontal gyrus, medial orbital    | PUT          | Lenticular nucleus, putamen                           |
| MFG          | Middle frontal gyrus                      | REC          | Gyrus rectus  |
| ORBmid       | Middle frontal gyrus, orbital part        | ROL          | Rolandic operculum                                    |
| SFGdor       | Superior frontal gyrus, dorsolateral      | SMA          | Supplementary motor area                              |
| SFGmed       | Superior frontal gyrus, medial            | SMG          | Supramarginal gyrus                                   |
| ORBsup       | Superior frontal gyrus, orbital part      | ITG          | Inferior temporal gyrus                               |
| FFG          | Fusiform gyrus                            | MTG          | Middle temporal gyrus                                 |
| HES          | Heschl gyrus                              | TPOmid       | Temporal pole: middle temporal gyrus                  |
| HIP          | Hippocampus                               | TPOsup       | Temporal pole: superior temporal gyrus                |
| INS          | Insula                                    | STG          | Superior temporal gyrus                               |
| LING         | Lingual gyrus                             | THA          | Thalamus  |
| IOG          | Inferior occipital gyrus                  |              |   |

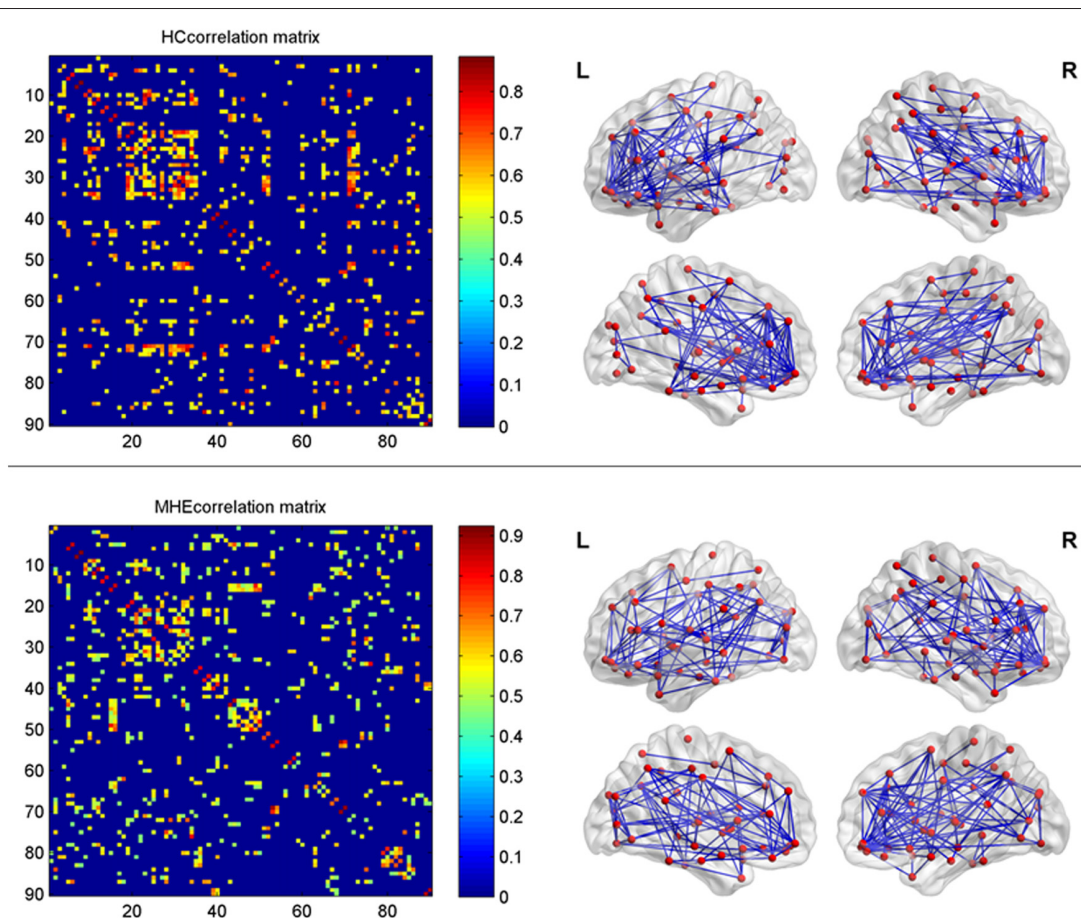


**FIGURE 1 |** The interregional correlations matrix in healthy control (HC) and minimal hepatic encephalopathy (MHE) groups. The color bar represents correlation strength. These matrices indicate the maps thresholded at the minimum network density (=12%), wherein the networks depicted full connectivity (without fragmented nodes). The region number (from 1 to 90) represents automated anatomical labeling (AAL) areas, including AMYG.L(R), ANG.L(R), CAL.L(R), CAU.L(R), ACG.L(R), DCG.L(R), PCG.L(R), CUN.L(R), IFGoperc.L(R), ORBinf.L(R), IFGtriang.L(R), ORBsupmed.L(R), MFG.L(R), ORBmid.L(R), SFGdor.L(R), SFGmed.L(R), ORBsup.L(R), FFG.L(R), HES.L(R), HIP.L(R), INS.L(R), LING.L(R), IOG.L(R), MOG.L(R), SOG.L(R), OLF.L(R), PAL.L(R), PCL.L(R), PHG.L(R), IPL.L(R), SPG.L(R), PoCG.L(R), PreCG.L(R), PCUN.L(R), PUT.L(R), REC.L(R), ROL.L(R), SMA.L(R), SMG.L(R), ITG.L(R), MTG.L(R), TPomid.L(R), TPOsup.L(R), STG.L(R), and THA.L(R). L and R indicate the left and right side, respectively. The right panel shows the graphical representation of the corresponding brain connectivity. The abbreviations for brain regions are presented in **Table 2**.

(range: 0.12–0.50, with interval = 0.02; Singh et al., 2013). The minimum density was determined to guarantee that the brain structural network of the two groups was fully connected. For density >0.5, the network exhibited a higher degree of randomness (small-world index  $\sim 1.0$ ; Singh et al., 2013). Finally, the graph theoretical methods were performed to analyze the resulting networks.

### Graph Theoretical Analysis

The Graph Analysis Toolbox (Hosseini et al., 2012), which integrates the Brain Connectivity Toolbox by Sporns and Rubinov for the quantification of network measures, was used in graph theoretical analysis.

To characterize the topological properties of brain structural networks, several key metrics were calculated, including the clustering coefficient ( $C_p$ ), characteristic path length ( $L_p$ ), and small-world parameters (i.e., normalized clustering coefficient

( $\gamma$ ), normalized path length ( $\lambda$ ), and small-worldness ( $\sigma$ ); Watts and Strogatz, 1998; Rubinov and Sporns, 2010).  $C_p$  is the average clustering coefficients across all nodes of a network, wherein the clustering coefficient  $C_i$  of a node  $i$  pertains to the number of existing connections linking the neighbors of the node divided by all their possible connections. The  $L_p$  of a network pertains to the average distance of the shortest path involving all node pairs within the network, in which the shortest path represents the number of edges that connects two nodes. Previous studies have shown that brain functional and structural networks exhibit efficient small-world properties that allow the efficient transfer of parallel information using a relatively low cost (Watts and Strogatz, 1998; Achard and Bullmore, 2007; He et al., 2007). Thus, a brain network that features small-world properties possesses a higher  $C_p$  yet similar  $L_p$  compared to the null random networks (Watts and Strogatz, 1998), and a small-world network fulfills the

following criteria:  $\gamma = C_p^{\text{real}}/C_p^{\text{rand}} > 1$ ,  $\lambda = L_p^{\text{real}}/L_p^{\text{rand}} \sim 1$ , and  $\sigma = \gamma/\lambda > 1$ , in which  $C_p^{\text{rand}}$  and  $L_p^{\text{rand}}$  represent the average clustering coefficient and characteristic path length of the matching random networks, respectively. In the present study, null random networks (number = 20) were generated from covariance matrices that match the distributional features of the observed covariance matrix based on the Hirschberger-Qi-Steuer algorithm, as described in previous studies (Zalesky et al., 2012; Singh et al., 2013).

For regional characteristics, the present study considered nodal degree as well as betweenness. The degree of a given node pertains to the sum of all connections situated between this node and the rest of the other nodes within the network. The betweenness of a specific node is described as the number of the shortest paths between a pair of nodes that run through this particular node. In the present study, the quantified nodal degree and/or betweenness were normalized using the average degree and/or betweenness of the network, respectively, followed by a comparison of two groups (Hosseini et al., 2012; Singh et al., 2013). The network hubs are the nodes that commonly interact with various other regions and allow functional integration as well as play a key role in instilling network resilience to insults. The nodes are thus regarded as the structural network hubs when these depict a higher degree (one standard deviation higher than the average network degree). The analysis of the regional network and hub was performed on the network that was thresholded at the minimum density for full connectivity.

## Statistical Analyses

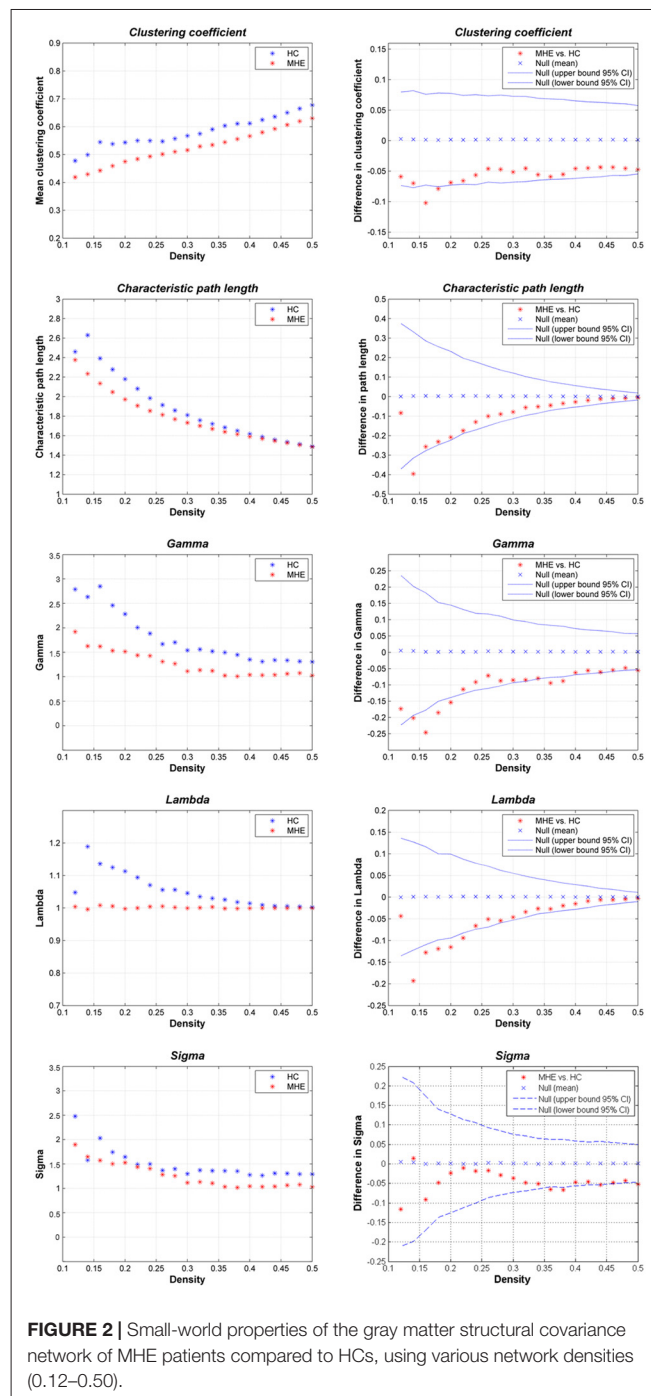
The Graph Analysis Toolbox was used to conduct a comparison of network measurements between two groups. To test differences in topological parameters between groups, a permutation-based algorithm was employed (Bullmore et al., 1999; He et al., 2008). Here, a set of corrected RGMV data of one individual was randomly rearranged to that of another subject of any group, and then the correlation matrix was computed for the randomized group. Subsequently, a new binarized matrix was generated using a density threshold similar to that of real brain networks, followed by recalculation of the network parameters. We repeated this randomization procedure for 1,000 times using each threshold (density). Then, we computed for the network measures of all the networks at every density. We also calculated the differences in network measures among the newly randomized groups (using various network densities), thereby resulting in a difference permutation distribution under the null hypothesis. The entire set of 95 percentile points of every distribution was employed as the critical values in a one-tailed test of the null hypothesis using a type I error probability of 0.05.

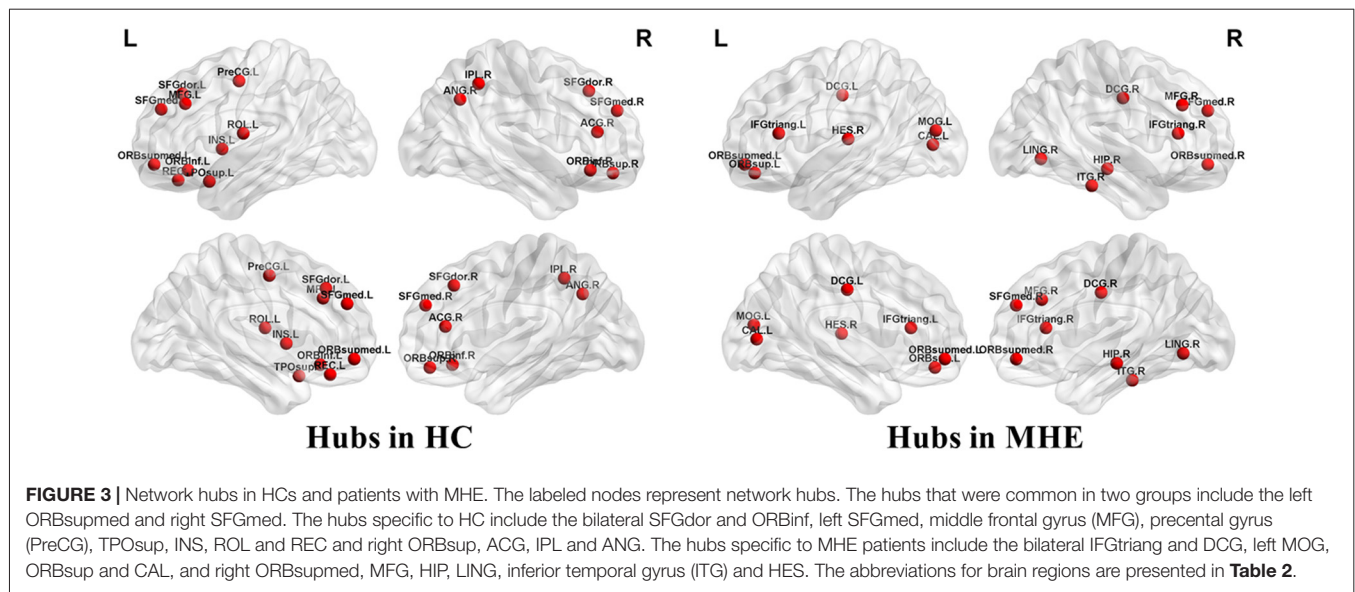
In addition, the functional data analysis (FDA) was conducted to examine MHE-related differences in topological metrics. Here, we computed the sum of between-group differences in every network metric within a range of densities (0.12–0.50) that can be used as a summary scale for the topological assessment of brain structural networks, which does not require single-threshold selection. Subsequently, we performed a nonparametric permutation test using the FDA results to

examine the significance of differences among groups (i.e., the observed summation).

## RESULTS

Figure 2 shows that the HC group demonstrated small-world network properties, i.e., considerable larger clustering coefficients and similar path lengths than those of the matched random networks. MHE patients showed lower  $C_p$ ,  $L_p$ ,  $\gamma$ ,  $\lambda$  and  $\sigma$ . Statistically, FDA analysis indicated that MHE patients





had significantly lower  $\gamma$  ( $P = 0.021$ ),  $\lambda$  ( $P = 0.010$ ) and  $\sigma$  ( $P = 0.048$ ). For the non-normalized network measures, FDA analysis also indicated that the MHE group had decreased  $C_p$  ( $P = 0.030$ ) and  $L_p$  ( $P = 0.043$ ), as compared with HC group.

**Figure 3** shows the hubs identified in each group. The number of hubs in the MHE group was less than that in the HC group. In the HC group, 17 regions were designated as network hubs, including eight association regions, eight

**TABLE 3 |** List of network hubs.

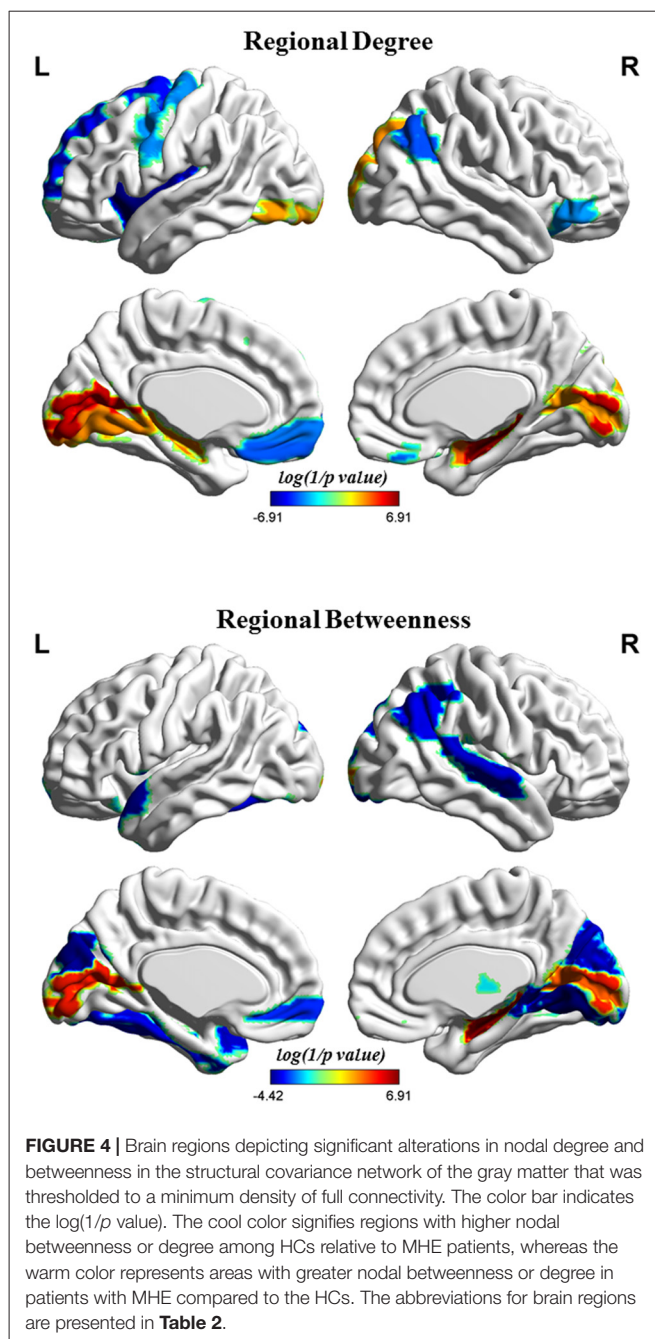
| Abbreviation             | AAL region  | Functional classification | Anatomical classification |
|--------------------------|---|---------------------------|---------------------------|
| <b>Hubs in HC group</b>  |   |                           |                           |
| ACG.R                    | Right anterior cingulate and paracingulate gyri             | Paralimbic                | Prefrontal                |
| ANG.R                    | Right angular gyrus   | Association               | Parietal                  |
| INS.L                    | Left insula   | Paralimbic                | Subcortical               |
| IPL.R                    | Right inferior parietal, but supramarginal and angular gyri | Association               | Parietal                  |
| MFG.L                    | Left middle frontal gyrus                                   | Association               | Prefrontal                |
| ORBinf.L                 | Left inferior frontal gyrus, orbital part                   | Paralimbic                | Prefrontal                |
| ORBinf.R                 | Right inferior frontal gyrus, orbital part                  | Paralimbic                | Prefrontal                |
| ORBsup.R                 | Right superior frontal gyrus, orbital part                  | Paralimbic                | Prefrontal                |
| ORBsupmed.L              | Left superior frontal gyrus, medial orbital                 | Paralimbic                | Prefrontal                |
| PreCG.L                  | Left precentral gyrus                                       | Primary                   | Frontal                   |
| REC.L                    | Left gyrus rectus   | Paralimbic                | Prefrontal                |
| ROL.L                    | Left rolandic operculum                                     | Association               | Frontal                   |
| SFGdor.L                 | Left superior frontal gyrus, dorsolateral                   | Association               | Prefrontal                |
| SFGdor.R                 | Right superior frontal gyrus, dorsolateral                  | Association               | Prefrontal                |
| SFGmed.L                 | Left superior frontal gyrus, medial                         | Association               | Prefrontal                |
| SFGmed.R                 | Right superior frontal gyrus, medial                        | Association               | Prefrontal                |
| TPOsup.L                 | Left temporal pole: superior temporal gyrus                 | Paralimbic                | Temporal                  |
| <b>Hubs in MHE group</b> |   |                           |                           |
| CAL.L                    | Left calcarine fissure and surrounding cortex               | Primary                   | Occipital                 |
| DCG.L                    | Left median cingulate and paracingulate gyri                | Paralimbic                | Frontal                   |
| DCG.R                    | Right median cingulate and paracingulate gyri               | Paralimbic                | Frontal                   |
| HES.R                    | Right heschl gyrus  | Primary                   | Temporal                  |
| HIP.R                    | Right hippocampus   | Limbic                    | Temporal                  |
| IFGtriang.L              | Left inferior frontal gyrus, triangular part                | Association               | Prefrontal                |
| IFGtriang.R              | Right inferior frontal gyrus, triangular part               | Association               | Prefrontal                |
| ITG.R                    | Right inferior temporal gyrus                               | Association               | Temporal                  |
| LING.R                   | Right lingual gyrus   | Association               | Occipital                 |
| MFG.R                    | Right middle frontal gyrus                                  | Association               | Prefrontal                |
| MOG.L                    | Left middle occipital gyrus                                 | Association               | Occipital                 |
| ORBsup.L                 | Left superior frontal gyrus, orbital part                   | Paralimbic                | Prefrontal                |
| ORBsupmed.L              | Left superior frontal gyrus, medial orbital                 | Paralimbic                | Prefrontal                |
| ORBsupmed.R              | Right superior frontal gyrus, medial orbital                | Paralimbic                | Prefrontal                |
| SFGmed.R                 | Right superior frontal gyrus, medial                        | Association               | Prefrontal                |

limbic/paralimbic regions, and one primary region. These were primarily located in the prefrontal, parietal, insular and motor areas, which are involved in the executive control, default-mode, salience and motor networks (Barkhof et al., 2014). These hubs identified in our study agree with those of previous reports (Singh et al., 2013). The 15 hubs were identified in the MHE group, including seven association regions, six limbic/paralimbic regions, and two primary regions. These hubs were primarily in frontal/prefrontal, temporal, and occipital areas. All hubs in two groups are listed in **Table 3**. The hubs that were common in two groups include the left ORBsupmed and right SFGmed. The hubs specific to HC include the bilateral SFGdor and ORBinf, left SFGmed, middle frontal gyrus (MFG), precentral gyrus (PreCG), TPOsup, INS, ROL and REC and right ORBsup, ACG, IPL and angular gyrus (ANG). The hubs specific to MHE patients include the bilateral IFGtriang and DCG, left MOG, ORBsup and CAL, and right ORBsupmed, MFG, HIP, LING, inferior temporal gyrus (ITG) and HES.

**Figure 4** shows the differences in regional network properties between two groups. Several brain regions with significant alterations in nodal degree and betweenness were detected in the structural covariance network of the gray matter that was thresholded to a minimum density of full connectivity. Compared to HC, the MHE group showed significantly lower nodal degree in the left SFGdor, ORBsupmed, PreCG, INS and REC and right ANG and ORBinf, whereas MHE patients had higher nodal degree in bilateral CAL and HIP, left LING and inferior occipital gyrus (IOG), and right superior occipital gyrus (SOG) and AMYG. In addition, the MHE patients showed significantly decreased nodal betweenness in bilateral CUN, left ORBsupmed, Fusiform gyrus (FFG) and TPOsup, and right ANG, IPL, LING, superior temporal gyrus (STG) and THA, and the MHE patients had significantly increased nodal betweenness in bilateral CAL and right HIP.

## DISCUSSION

This study serves as the first investigation of the complex topological organization of brain structural networks in cirrhotic patients with MHE. Our results suggest that MHE patients exhibit an unoptimizable architecture involving the gray matter structural covariance network, as indicated by reduced clustering coefficients and characteristic path lengths and lower small-worldness parameters. These changes indicated a tendency to undergo additional random alterations in the brain structural network of patients with MHE, which shows less efficient communication of information across the whole brain. Similar to our results, a previous study has also revealed an anomalous gray matter structural network (with a decreased clustering coefficient and small-worldness) in the patients with cirrhosis (but only a few could be diagnosed as MHE; Lv et al., 2015). Thus, our findings provide morphological evidence that supports the concept that MHE is a neuropathological process associated with disruptive alterations to brain networks.



Previous analyses of functional connectivity networks have revealed that the neurocognitive deficiencies in MHE patients are associated with a deficiency in small-world properties, including more random and poor clustered architecture (Zhang et al., 2014; Jao et al., 2015). Studies have shown that the functionally linked networks reflect the underlying organization relating to the brain's structural connectivity (van den Heuvel et al., 2009), and brain structural connectivity supports the functional network organization and various functional network graph features (Honey et al., 2009; Zimmermann et al., 2016). Therefore, it is expected that MHE patients have impaired topological organization in the brain structural covariance network, which

may be considered as the neural substrate for the dysfunction of functional brain networks that subsequently contribute to neurocognitive impairment. The findings of this study indicate that the brain structural covariance network exhibits a more randomized configuration with lower  $C_p$ , higher  $L_p$ , as well as lower  $\sigma$  (Watts and Strogatz, 1998; Bullmore and Sporns, 2009) in patients with MHE, which agrees well with the results of earlier functional investigations (Zhang et al., 2014; Jao et al., 2015). The random networks involve fewer modularized information processing or tolerance of faults relative to small-world networks (Latora and Marchiori, 2001). Therefore, this explains why MHE leads to impaired small-world network efficiency functionality (Hsu et al., 2012), which indicates less efficient informational interactions between interconnected brain regions. Meanwhile, less fault-tolerance may imply an increase in vulnerability to cerebral metabolic disturbances (such as hyperammonemia-related edema and neurotoxic manganese deposition; Rovira et al., 2008) due to liver dysfunction. That may be the reason why once the disease gets to the stage of MHE, it is likely to progress to overt hepatic encephalopathy (HE), which has poor prognosis (Romero-Gómez et al., 2001; Stewart et al., 2007).

MHE patients had fewer hubs than those in the HC group (15 vs. 17) and showed a different distribution of network hubs from the HC group. They lost hub nodes mainly from the bilateral frontal lobe, right parietal lobe, as well as the left insular cortex, which are areas that are most frequently affected in MHE (Hsu et al., 2012; Zhang et al., 2012; Chen et al., 2013; Yang et al., 2018). Thus, our finding further indicated the selective vulnerability of these areas in the case of MHE. Although the mechanism about the loss of these hubs was not well understood, several pathological processes in MHE may contribute to the functional and structural alterations in these areas. For example, it could be implied that the alteration in cortical hub may be associated with the consequence of subcortical pathology (basal ganglia and cerebellum) due to hepatic dysfunction. The previous study has revealed abnormal cerebral blood flow/glucose metabolism in MHE, which is attributable to a redistribution of cerebral blood flow/glucose metabolism from the cortex to the caudate, thalamus, and cerebellum. Of note, the above hub-regions are considered as critical nodes that are responsible for high-level cognitive networks, such as executive activities, default-mode, as well as salience (Barkhof et al., 2014; Chen et al., 2016). Consistently, the reduction in nodal degree/betweenness in MHE was also found in the above networks. Therefore, the loss of these hubs may contribute to the common cognitive decline in MHE, such as executive dysfunction and attention deficit (Bajaj et al., 2009). However, the MHE group had new hubs, primarily located in the bilateral occipital lobe and right temporal lobe; consistently, they showed an increased degree/betweenness primarily in bilateral calcarine fissure and the surrounding cortex and bilateral hippocampus. As mentioned in previous studies (Hsu et al., 2012; Lv et al., 2015), these alterations implied the possibility that several hubs/nodes in the brain structural network undergo reorganization and compensate for the MHE-related declines in neurological function, such as visuo-

spatial coordination and memory abilities (Ortiz et al., 2006; Bajaj et al., 2013; Ciećko-Michalska et al., 2013). This compensation mechanism would be helpful to delay the progression of HE disease.

This study has a number of limitations. First, we conducted a cross-sectional study. Future studies with longitudinal evaluation are recommended to directly test the progressive effects of HE on the topological properties of brain structural networks. Second, the topological measurements of the brain structural network can be identified by calculating the interregional correlations of RGMV among the participants in each group. The drawback of this approach in constructing a brain network is that it prevents the assessment of individual differences within network metrics, thereby making it difficult to explore the impact of unoptimizable network organization on MHE-related cognitive-behavioral outcomes. Third, the present study only assessed the topological features of the structural covariance network of the gray matter. The integrated analysis of functional as well as structural connectivity networks may generate novel insights into investigating the complex network properties of both healthy and diseased brains (Damoiseaux and Greicius, 2009; Zhang et al., 2011). Therefore, the further investigations involving multi-modal data, including T1-weighted, diffusion-based, as well as resting-state functional magnetic resonance images, should be performed to improve our knowledge of the topological features of complex brain networks in early stage HE.

In summary, our results revealed that MHE leads to the altered coordination patterns involving gray matter morphology. The loss of small-world topological features indicated a less efficient network organization even during the early stages of HE. The randomization alteration is an important characteristic occurring in the whole-brain network of MHE patients, which may contribute to the various neurological deficits, such as executive and attention dysfunction, and the motor and visual impairments. Our findings provide structural evidence that supports that MHE is a neurological complication related to disrupted neural networks.

## AUTHOR CONTRIBUTIONS

H-JC, T-XZ and LS conceived and designed the study, acquired and analyzed the data and wrote the manuscript. H-JC, CZ and Y-QG contributed to data analysis. All authors have read and approved the manuscript.

## ACKNOWLEDGMENTS

This study was funded by the grants from the National Natural Science Foundation of China (Grant No. 81501450), Fujian Provincial Science Fund for Distinguished Young Scholars (Grant No. 2018J06023), Fujian Provincial Program for Distinguished Young Scholars (Grant No. 2017B023), and Fujian Provincial Health Commission Project for Scientific Research Talents (Grant No. 2018-ZQN-28).

## REFERENCES

- Achard, S., and Bullmore, E. (2007). Efficiency and cost of economical brain functional networks. *PLoS Comput. Biol.* 3:e17. doi: 10.1371/journal.pcbi.0030017
- Amodio, P., Pellegrini, A., Amistà, P., Luise, S., Del Piccolo, F., Mapelli, D., et al. (2003). Neuropsychological-neurophysiological alterations and brain atrophy in cirrhotic patients. *Metab. Brain Dis.* 18, 63–78. doi: 10.1023/A:1021982719654
- Ashburner, J. (2007). A fast diffeomorphic image registration algorithm. *Neuroimage* 38, 95–113. doi: 10.1016/j.neuroimage.2007.07.007
- Bajaj, J. S., Thacker, L. R., Heuman, D. M., Fuchs, M., Sterling, R. K., Sanyal, A. J., et al. (2013). The stroop smartphone application is a short and valid method to screen for minimal hepatic encephalopathy. *Hepatology* 58, 1122–1132. doi: 10.1002/hep.26309
- Bajaj, J. S., Wade, J. B., and Sanyal, A. J. (2009). Spectrum of neurocognitive impairment in cirrhosis: implications for the assessment of hepatic encephalopathy. *Hepatology* 50, 2014–2021. doi: 10.1002/hep.23216
- Barkhof, F., Haller, S., and Rombouts, S. A. (2014). Resting-state functional MR imaging: a new window to the brain. *Radiology* 272, 29–49. doi: 10.1148/radiol.14132388
- Bhojraj, T. S., Prasad, K. M., Eack, S. M., Francis, A. N., Montrose, D. M., and Keshavan, M. S. (2010). Do inter-regional gray-matter volumetric correlations reflect altered functional connectivity in high-risk offspring of schizophrenia patients? *Schizophr. Res.* 118, 62–68. doi: 10.1016/j.schres.2010.01.019
- Bullmore, E., and Sporns, O. (2009). Complex brain networks: graph theoretical analysis of structural and functional systems. *Nat. Rev. Neurosci.* 10, 186–198. doi: 10.1038/nrn2575
- Bullmore, E. T., Suckling, J., Overmeyer, S., Rabe-Hesketh, S., Taylor, E., and Brammer, M. J. (1999). Global, voxel and cluster tests, by theory and permutation, for a difference between two groups of structural MR images of the brain. *IEEE Trans. Med. Imaging* 18, 32–42. doi: 10.1109/42.750253
- Butterworth, R. F. (2007). Neuronal cell death in hepatic encephalopathy. *Metab. Brain Dis.* 22, 309–320. doi: 10.1007/s11011-007-9072-3
- Chen, H.-J., Chen, Q.-F., Liu, J., and Shi, H.-B. (2016). Aberrant salience network and its functional coupling with default and executive networks in minimal hepatic encephalopathy: a resting-state fMRI study. *Sci. Rep.* 6:27092. doi: 10.1038/srep27092
- Chen, H.-J., Jiang, L.-F., Sun, T., Liu, J., Chen, Q.-F., and Shi, H.-B. (2015). Resting-state functional connectivity abnormalities correlate with psychometric hepatic encephalopathy score in cirrhosis. *Eur. J. Radiol.* 84, 2287–2295. doi: 10.1016/j.ejrad.2015.08.005
- Chen, H.-J., Jiao, Y., Zhu, X.-Q., Zhang, H. Y., Liu, J.-C., Wen, S., et al. (2013). Brain dysfunction primarily related to previous overt hepatic encephalopathy compared with minimal hepatic encephalopathy: resting-state functional MR imaging demonstration. *Radiology* 266, 261–270. doi: 10.1148/radiol.12120026
- Ciećko-Michalska, I., Wójcik, J., Senderecka, M., Wyczesany, M., Binder, M., Szewczyk, J., et al. (2013). Cognitive functions in patients with liver cirrhosis: a tendency to commit more memory errors. *Med. Sci. Monit.* 19, 283–288. doi: 10.12659/msm.883890
- Damoiseaux, J. S., and Greicius, M. D. (2009). Greater than the sum of its parts: a review of studies combining structural connectivity and resting-state functional connectivity. *Brain Struct. Funct.* 213, 525–533. doi: 10.1007/s00429-009-0208-6
- Dazzan, P., Morgan, K. D., Orr, K. G., Hutchinson, G., Chitnis, X., Suckling, J., et al. (2004). The structural brain correlates of neurological soft signs in AESOP first-episode psychoses study. *Brain* 127, 143–153. doi: 10.1093/brain/awh015
- Guevara, M., Baccaro, M. E., Gómez-Anson, B., Frisoni, G., Testa, C., Torre, A., et al. (2011). Cerebral magnetic resonance imaging reveals marked abnormalities of brain tissue density in patients with cirrhosis without overt hepatic encephalopathy. *J. Hepatol.* 55, 564–573. doi: 10.1016/j.jhep.2010.12.008
- He, Y., Chen, Z. J., and Evans, A. C. (2007). Small-world anatomical networks in the human brain revealed by cortical thickness from MRI. *Cereb. Cortex* 17, 2407–2419. doi: 10.1093/cercor/bhl149
- He, Y., Chen, Z., and Evans, A. (2008). Structural insights into aberrant topological patterns of large-scale cortical networks in Alzheimer's disease. *J. Neurosci.* 28, 4756–4766. doi: 10.1523/JNEUROSCI.0141-08.2008
- He, Y., Dagher, A., Chen, Z., Charil, A., Zijdenbos, A., Worsley, K., et al. (2009). Impaired small-world efficiency in structural cortical networks in multiple sclerosis associated with white matter lesion load. *Brain* 132, 3366–3379. doi: 10.1093/brain/awp089
- Honey, C. J., Sporns, O., Cammoun, L., Gigandet, X., Thiran, J. P., Meuli, R., et al. (2009). Predicting human resting-state functional connectivity from structural connectivity. *Proc. Natl. Acad. Sci. U S A* 106, 2035–2040. doi: 10.1073/pnas.0811168106
- Hosseini, S. M., Hoefl, F., and Kesler, S. R. (2012). GAT: a graph-theoretical analysis toolbox for analyzing between-group differences in large-scale structural and functional brain networks. *PLoS One* 7:e40709. doi: 10.1371/journal.pone.0040709
- Hsu, T.-W., Wu, C. W., Cheng, Y.-F., Chen, H.-L., Lu, C.-H., Cho, K.-H., et al. (2012). Impaired small-world network efficiency and dynamic functional distribution in patients with cirrhosis. *PLoS One* 7:e35266. doi: 10.1371/journal.pone.0035266
- Iwasa, M., Mifujii-Moroka, R., Kuroda, M., Moroka, H., Fujita, N., Kobayashi, Y., et al. (2012). Regional reduction in gray and white matter volume in brains of cirrhotic patients: voxel-based analysis of MRI. *Metab. Brain Dis.* 27, 551–557. doi: 10.1007/s11011-012-9314-x
- Jao, T., Schröter, M., Chen, C. L., Cheng, Y. F., Lo, C. Y., Chou, K. H., et al. (2015). Functional brain network changes associated with clinical and biochemical measures of the severity of hepatic encephalopathy. *Neuroimage* 122, 332–344. doi: 10.1016/j.neuroimage.2015.07.068
- Krill, J. J., and Butterworth, R. F. (1997). Diencephalic and cerebellar pathology in alcoholic and nonalcoholic patients with end-stage liver disease. *Hepatology* 26, 837–841. doi: 10.1002/hep.510260405
- Latora, V., and Marchiori, M. (2001). Efficient behavior of small-world networks. *Phys. Rev. Lett.* 87:198701. doi: 10.1103/PhysRevLett.87.198701
- Lv, B., Li, J., He, H., Li, M., Zhao, M., Ai, L., et al. (2010). Gender consistency and difference in healthy adults revealed by cortical thickness. *Neuroimage* 53, 373–382. doi: 10.1016/j.neuroimage.2010.05.020
- Lv, X.-F., Liu, K., Qiu, Y.-W., Cai, P.-Q., Li, J., Jiang, G.-H., et al. (2015). Anomalous gray matter structural networks in patients with hepatitis B virus-related cirrhosis without overt hepatic encephalopathy. *PLoS One* 10:e0119339. doi: 10.1371/journal.pone.0119339
- Montoliu, C., Gonzalez-Escamilla, G., Atienza, M., Urios, A., Gonzalez, O., Wassel, A., et al. (2012). Focal cortical damage parallels cognitive impairment in minimal hepatic encephalopathy. *Neuroimage* 61, 1165–1175. doi: 10.1016/j.neuroimage.2012.03.041
- Ortiz, M., Córdoba, J., Jacas, C., Flavia, M., Esteban, R., and Guardia, J. (2006). Neuropsychological abnormalities in cirrhosis include learning impairment. *J. Hepatol.* 44, 104–110. doi: 10.1016/j.jhep.2005.06.013
- Qi, R., Zhang, L. J., Xu, Q., Zhong, J., Wu, S., Zhang, Z., et al. (2012). Selective impairments of resting-state networks in minimal hepatic encephalopathy. *PLoS One* 7:e37400. doi: 10.1371/journal.pone.0037400
- Romero-Gómez, M., Boza, F., García-Valdecasas, M. S., García, E., and Aguilar-Reina, J. (2001). Subclinical hepatic encephalopathy predicts the development of overt hepatic encephalopathy. *Am. J. Gastroenterol.* 96, 2718–2723. doi: 10.1111/j.1572-0241.2001.04130.x
- Rovira, A., Alonso, J., and Córdoba, J. (2008). MR imaging findings in hepatic encephalopathy. *AJNR Am. J. Neuroradiol.* 29, 1612–1621. doi: 10.3174/ajnr.A1139
- Rubinov, M., and Sporns, O. (2010). Complex network measures of brain connectivity: uses and interpretations. *Neuroimage* 52, 1059–1069. doi: 10.1016/j.neuroimage.2009.10.003
- Shi, F., Yap, P. T., Gao, W., Lin, W., Gilmore, J. H., and Shen, D. (2012). Altered structural connectivity in neonates at genetic risk for schizophrenia: a combined study using morphological and white matter networks. *Neuroimage* 62, 1622–1633. doi: 10.1016/j.neuroimage.2012.05.026
- Singh, M. K., Kesler, S. R., Hadi Hosseini, S. M., Kelley, R. G., Amatya, D., Hamilton, J. P., et al. (2013). Anomalous gray matter structural networks in major depressive disorder. *Biol. Psychiatry* 74, 777–785. doi: 10.1016/j.biopsych.2013.03.005
- Sporns, O., Tononi, G., and Kötter, R. (2005). The human connectome: a structural description of the human brain. *PLoS Comput. Biol.* 1:e42. doi: 10.1371/journal.pcbi.0010042

- Stewart, C. A., Malinchoc, M., Kim, W. R., and Kamath, P. S. (2007). Hepatic encephalopathy as a predictor of survival in patients with end-stage liver disease. *Liver Transpl.* 13, 1366–1371. doi: 10.1002/lt.21129
- Stewart, C. A., and Smith, G. E. (2007). Minimal hepatic encephalopathy. *Nat. Clin. Pract. Gastroenterol. Hepatol.* 4, 677–685. doi: 10.1038/ncpgasthep0999
- Tarter, R. E., Hays, A. L., Sandford, S. S., and Van Thiel, D. H. (1986). Cerebral morphological abnormalities associated with non-alcoholic cirrhosis. *Lancet* 2, 893–895. doi: 10.1016/s0140-6736(86)90413-7
- Tzourio-Mazoyer, N., Landeau, B., Papathanassiou, D., Crivello, F., Etard, O., Delcroix, N., et al. (2002). Automated anatomical labeling of activations in SPM using a macroscopic anatomical parcellation of the MNI MRI single-subject brain. *Neuroimage* 15, 273–289. doi: 10.1006/nimg.2001.0978
- van den Heuvel, M. P., Mandl, R. C., Kahn, R. S., and Hulshoff Pol, H. E. (2009). Functionally linked resting-state networks reflect the underlying structural connectivity architecture of the human brain. *Hum. Brain Mapp.* 30, 3127–3141. doi: 10.1002/hbm.20737
- Watts, D. J., and Strogatz, S. H. (1998). Collective dynamics of ‘small-world’ networks. *Nature* 393, 440–442. doi: 10.1038/30918
- Wen, W., He, Y., and Sachdev, P. (2011). Structural brain networks and neuropsychiatric disorders. *Curr. Opin. Psychiatry* 24, 219–225. doi: 10.1097/YCO.0b013e32834591f8
- Wu, K., Taki, Y., Sato, K., Kinomura, S., Goto, R., Okada, K., et al. (2012). Age-related changes in topological organization of structural brain networks in healthy individuals. *Hum. Brain Mapp.* 33, 552–568. doi: 10.1002/hbm.21232
- Yang, Z.-T., Chen, H.-J., Chen, Q.-F., and Lin, H. (2018). Disrupted brain intrinsic networks and executive dysfunction in cirrhotic patients without overt hepatic encephalopathy. *Front. Neurol.* 9:14. doi: 10.3389/fneur.2018.00014
- Yao, Z., Zhang, Y., Lin, L., Zhou, Y., Xu, C., Jiang, T., et al. (2010). Abnormal cortical networks in mild cognitive impairment and Alzheimer’s disease. *PLoS Comput. Biol.* 6:e1001006. doi: 10.1371/journal.pcbi.1001006
- Zalesky, A., Fornito, A., and Bullmore, E. (2012). On the use of correlation as a measure of network connectivity. *Neuroimage* 60, 2096–2106. doi: 10.1016/j.neuroimage.2012.02.001
- Zeneroli, M. L., Cioni, G., Crisi, G., Vezzelli, C., and Ventura, E. (1991). Globus pallidus alterations and brain atrophy in liver cirrhosis patients with encephalopathy: an MR imaging study. *Magn. Reson. Imaging* 9, 295–302. doi: 10.1016/0730-725x(91)90414-h
- Zeneroli, M. L., Cioni, G., Vezzelli, C., Grandi, S., Crisi, G., Luzietti, R., et al. (1987). Prevalence of brain atrophy in liver cirrhosis patients with chronic persistent encephalopathy. *J. Hepatol.* 4, 283–292. doi: 10.1016/s0168-8278(87)80536-6
- Zhang, Z., Liao, W., Chen, H., Mantini, D., Ding, J. R., Xu, Q., et al. (2011). Altered functional-structural coupling of large-scale brain networks in idiopathic generalized epilepsy. *Brain* 134, 2912–2928. doi: 10.1093/brain/awr223
- Zhang, L. J., Zheng, G., Zhang, L., Zhong, J., Li, Q., Zhao, T. Z., et al. (2014). Disrupted small world networks in patients without overt hepatic encephalopathy: a resting state fMRI study. *Eur. J. Radiol.* 83, 1890–1899. doi: 10.1016/j.ejrad.2014.06.019
- Zhang, L. J., Zheng, G., Zhang, L., Zhong, J., Wu, S., Qi, R., et al. (2012). Altered brain functional connectivity in patients with cirrhosis and minimal hepatic encephalopathy: a functional MR imaging study. *Radiology* 265, 528–536. doi: 10.1148/radiol.12120185
- Zhu, W., Wen, W., He, Y., Xia, A., Anstey, K. J., and Sachdev, P. (2012). Changing topological patterns in normal aging using large-scale structural networks. *Neurobiol. Aging* 33, 899–913. doi: 10.1016/j.neurobiolaging.2010.06.022
- Zimmermann, J., Ritter, P., Shen, K., Rothmeier, S., Schirner, M., and McIntosh, A. R. (2016). Structural architecture supports functional organization in the human aging brain at a regionwise and network level. *Hum. Brain Mapp.* 37, 2645–2661. doi: 10.1002/hbm.23200

**Conflict of Interest Statement:** The authors declare that the research was conducted in the absence of any commercial or financial relationships that could be construed as a potential conflict of interest.

Copyright © 2018 Zou, She, Zhan, Gao and Chen. This is an open-access article distributed under the terms of the Creative Commons Attribution License (CC BY). The use, distribution or reproduction in other forums is permitted, provided the original author(s) and the copyright owner(s) are credited and that the original publication in this journal is cited, in accordance with accepted academic practice. No use, distribution or reproduction is permitted which does not comply with these terms.